A THREE-DIMENSIONAL STOCHASTIC SPATIO-TEMPORAL MODEL OF ISOTROPIC CELL SPREADING

Yuguang Xiong[1*], Padmini Rangamani[1*], Benjamin Dubin-Thaler[2], Michael P. Sheetz[2], Ravi Iyengar[1]

[1]Department of Pharmacology and Systems Therapeutics, Mount Sinai School of Medicine, New York, NY 10029

[2]Department of Biological Sciences, Columbia University, New York NY 10027

Address correspondence to

Ravi Iyengar

Department of Pharmacology and Systems Therapeutics, Box 1215

Mount Sinai School of Medicine

One Gustave Levy Place

New York NY 10029

Phone: 212-659-1707

Fax: 212-831-0114

E-mail: ravi.iyengar@mssm.edu

* These authors contributed equally to this work

Running Title: Stochastic spatio-temporal model of cell spreading

Abstract

Cell motility is important for many physiological processes and the underlying biochemical reactions motility have been well-characterized. Mathematical models, using the biochemical reactions and focused on different types of spreading behavior have been constructed and analyzed. In this study, we build on these previous models to develop a three-dimensional stochastic model of isotropic spreading of mammalian fibroblasts. The model is composed of three actin remodeling reactions that occur stochastically in space and time and are regulated by membrane resistance forces. Numerical simulations indicate that the model qualitatively captures the experimentally observed isotropic cell spreading behavior. We analyzed the effects of varying branching reaction rates, membrane resistance forces and capping protein concentrations on the dynamics of isotropic spreading. The simulations allowed us to identify the range within which branching reaction rates and membrane force values cooperate to yield isotropic spreading behavior. The model predicts increasing capping protein concentration would lead to a linear decrease in average peripheral velocity. We tested this prediction experimentally using varying concentrations of a pharmacologic agent (Cytochalasin D) that caps growing actin filaments. We find that the experimental results agree with the numerical simulations. Thus, a spatio-temporally complex model made up of a simple set of stochastic reactions near the cell surface, when constrained by membrane forces, can yield deterministic behavior as characterized by isotropic cell spreading.

Introduction

Cell motility plays an important role in many physiological processes including responses to infection and wound healing. In response to external stimuli, including both physical forces and chemical signals, cells reorganize their cytoskeleton in a dynamic fashion leading to cellular motility (1, 2). The processes underlying cell motility constitute some of the central functional processes at the cellular level and have been intensively studied both experimentally (3-5) and computationally (6-9). Spreading of cells on bioactive substrates has been a useful method to study cell motility. Experimental studies have described a number of phenomena that make up the various forms of cell motility (10-12). Although these descriptions of motility at the cellular leading edge are valuable, the observations made are mostly qualitative in nature. Moreover, these descriptions do not contain sufficient information to develop and constrain mechanistic computational models of whole cell motility. The development of TIRF microscopy has facilitated quantitative experimental approaches that measure directional spreading velocity (1, 12, 13). Spreading of fibroblasts on fibronectin coated glass surfaces can be imaged to obtain precise measurements of cell motility as defined by spatial distribution of velocity at the leading edge (1). This quantitative measure of integrated cell behavior provides valuable information to develop mechanistic computational models of how coupled biochemical reactions can lead to dynamic cell behavior. Even for relatively well-defined experimental situations such as isotropic cell spreading (1), the underlying process is complex.

Many informative computational models of actin polymerization-depolymerization cycles have been developed (4, 6, 8, 14, 15). Often these models are in

one spatial dimension and analyze the cytoskeletal reorganization process in an abstracted cytoskeletal structure at steady state. These models have yielded substantial insight into the dynamics of the underlying actin cytoskeleton and enable the development of models that explore the relationship between actin cytoskeleton dynamics and whole cell behavior such as cell spreading. A central question regarding this relationship is: will regulation of the core reactions of actin filament growth, branching and capping be sufficient to yield isotropic cell spreading? In this computational study, we sought to answer this question.

The minimal reactions required for actin cytoskeleton remodeling are actin polymerization, branching and capping at the leading edge. These reactions are regulated by both biochemical signals and plasma membrane defined physical forces. It is likely that the integration of physical and chemical signals around the perimeter of the cell determines spreading velocity and cell shape. The filament dynamics processes are stochastic, and explicit stochastic models would be more realistic and useful in determining how the underlying coupled biochemical reactions generate the observed dynamic phenotype. We hypothesized that the regulation of the actin filament remodeling reactions (polymerization, branching and capping) would be sufficient to generate dynamics similar to the experimentally observed behavior of fibroblasts spreading on fibronectin coated glass surfaces. We have developed a three-dimensional stochastic model of actin polymerization, branching, and capping regulated by membrane resistance forces and conducted numerical simulations to generate spatial velocity distributions of the leading edge during cell spreading. These studies show that biochemical regulation of the three reactions underlying actin filament dynamics, when integrated with regulation

by force to incorporate the physical properties of the plasma membrane, can account for the observed macroscopic behavior of cell spreading.

Results

The framework for the simulations is shown in Figure 1A and B, and a comparison of the cell surface in the model and experiments is shown in Figure 1C. Simulation results from the three-dimensional stochastic computational model were compared against experimental data for spreading of mouse fibroblasts on fibronectin coated slides (1). The initial concentrations of actin, Arp 2/3 and capping protein are 20 μM, 0.04 μM and 0.04 μM respectively. The membrane resistance force is maintained at 500 pN/μm^2. In Figure 2A, we show average spreading velocity distribution at the cell periphery averaged over 24 simulations. The spreading velocity ranges from 12.8 μm/min to -4 μm/min where the negative velocity indicates inward radial velocity toward the center of the cell (retraction). Figure 2B shows the experimentally observed velocity distribution at the cell periphery during the isotropic spreading stage.

In the case of isotropic spreading, we would expect that almost all spatial coordinates on the periphery of the cell exhibit similar velocities. Experimentally, isotropic cell spreading is characterized by a mean peripheral velocity of 3.4 ± 0.6 μm/min (1), indicating that a deviation of 20% from the mean is an acceptable value for the definition of isotropic spreading behavior. Therefore, for the simulations, we define isotropic spreading behavior as the case where the peripheral spreading velocity has a standard deviation of less than 20% from the mean. When we compare the spatial distribution of the spreading velocity across the periphery of the cell at four different times with the mean spreading velocity at that time, we find that at 5 seconds, the actual spreading velocity exhibits substantial deviations from the mean velocity along the cell periphery (Figure 2C). This deviation becomes smaller at longer times; at 20 and 40 seconds we see that most of the points lie close to the mean. There are a few spatial

coordinates (at 270 degrees, at 40 seconds) that exhibit a large deviation from the mean, indicative of the stochastic nature of the process. In the case of experimental observations, the early time points exhibit spreading that is not uniform along the cell periphery (5 and 10 seconds) but at 20 and 40 seconds, the spreading velocity distributions lie close to the mean values (Figure 2D). The stochastic nature of the spreading process is also evident in the experimental data at 40 seconds at the 120 degrees time point. In Figure S1, we show a series of snapshots of the spreading cell from our simulations at different times.

This comparison between simulations and experiments shows that we are able to capture isotropic cell spreading behavior in our model. However, the velocity in the simulations is substantially lower than that obtained experimentally. Since we do not know the spatially specified cellular concentrations of the components, we have not made an attempt to obtain quantitative matches of velocities between our simulation and the experiments. From the heat maps and the line graphs that show angular velocity as a function of time, it can be seen that simulations, like the experiments, show similar velocities around the cell periphery indicative of isotropic cell spreading.

Effect of the branching reaction

Concentrations of activated Arp 2/3 can directly affect spreading velocity distributions by controlling the branching of the actin filament network. We ran simulations with varying Arp 2/3 concentrations while keeping the concentrations of actin and capping protein constant at 20 μM and 0.04 μM respectively (Figure 3). We observe that as we increase the Arp2/3 concentration, the range of velocities does not change dramatically. However, there is a change in the distribution of the velocities. At

an Arp 2/3 concentration of 0.02 μM, a large part of the cell periphery spreads with a velocity close to 1 μm/min, with the maximum reaching 4 μm/min. At later times, there are pockets of cell periphery where the spreading velocity is close to zero indicated by blue in the heat map in Figure 3A. In the cases where Arp2/3 concentration is 0.08 and 0.16 μM, the velocity distribution contains fewer regions of zero or negative velocities (Figure 3B and 3C). Although the range of velocities is similar in these three cases, the spatial distribution of velocity tends toward isotropic spreading with increasing concentrations of Arp2/3. This suggests that increased branching ability of the filament network can lead to a spatially homogeneous behavior. The isotropic spreading velocity observed in experiments (in terms of uniform velocity distribution) (Figure 2B) is similar to that for 0.04 μM (Figure 2A) and 0.08 μM Arp 2/3 (Figure 3B). The increase in the spreading velocity caused by the increase of Arp2/3 concentration slows down as Arp2/3 concentration increases. This result is counter-intuitive because increased Arp2/3 concentration would be expected to further increase spreading velocity. However, this behavior can be explained by the relative probabilities of the elongation, branching and capping reactions. Normally, filament polymerization is dominant due to the large reaction rate constant and the high concentration of actin monomers making the rate of the filament polymerization reaction much larger than the rate of the other two reactions (Table 1 Supplementary material). This dominance of filament polymerization is required for maintaining an appropriate large ratio between filament polymerization rate and filament branching rate, such that filaments can grow fast enough to provide sufficient Arp2/3-binding sites for new filament branching. Another possibility is that increased Arp2/3 concentration may lead to a clash of the many branched filaments with the cell

surface resulting in decreased spreading velocity (Figure S5). The branching reaction may also be limited by the spatial restrictions imposed by the cell membrane and the number of branches on a preexisting filament.

Effect of the membrane resistance force

As first described by Mogilner and Oster (6), the membrane exerts a counter force on the actin filament dynamics. It is likely that this force is made up of several components including intrinsic membrane resistance, the force generated by membrane curvature and by attachment to the substrate. The contribution of these various force components in regulating cell spreading is beyond the scope of the present study. Since the exact value of the force exerted by the plasma membrane on the cytoskeleton in the context of isotopic cell spreading is not known, we used parameter variation to study the effect of different values of force on the cell spreading dynamics. The concentrations of actin, Arp2/3 and capping protein are maintained constant for these simulations at 20, 0.08, and 0.04 μM respectively. When the applied resistance force is zero, we see a large range of spreading velocities, with most spatial regions of the cell having a very small spreading velocity (Figure 4A). When there is no membrane resistance, there are sporadic instances of large spreading velocities and the remaining distribution is close to zero velocity. Although the force term appears as an exponential term only in equation (1), the spreading velocity distribution observed in Figure 4A indicates that force is a necessary component for cell spreading and the biochemical kinetics alone are not sufficient to capture the spreading behavior observed experimentally. Increasing values of resistance force leads to spreading behavior that is closer to isotropic spreading. However, the

increase in the value of force does not change the direction of filament elongation or branching. Table 1 shows the mean peripheral spreading velocity over 40 seconds and the standard deviation for different conditions of membrane resistance force and Arp2/3 concentration. For low resistance force (30 pN/μm^2 and 100 pN/μm^2), the spatial distribution of spreading velocities is not isotropic (Figure 4A and Table 1). We see positive spreading velocities for the first few seconds but observe large pockets of spreading velocity close to zero for a large part of the simulation time. When the membrane resistance force is maintained at 300 pN/μm^2 (Figure 4A, Table 1) we begin to see spreading velocity distributions that are similar to isotropic cell spreading behavior as observed in experiments (Figure 2B).

Using an experiment-derived definition for isotropic spreading, we find that the ability for this behavior is restricted to an identifiable set of conditions. We summarize the data in Table 1 as a phase diagram in the Arp2/3 concentration-membrane resistance force plane in Figure 4B. We find that low membrane force values (0, 30, 100 pN/μm^2) exhibit isotropic spreading behavior at low concentrations of Arp2/3 (0.02 μM). As membrane force increases (300, 500, 1000 pN/μm^2), isotropic spreading is observed for higher Arp2/3 concentrations (0.04, 0.08, 0.16 μM) and not at lower Arp2/3 concentration (0.02 μM). Identification of the exact combination of force and Arp2/3 conditions would require a detailed exploration of the parameter space of the problem and is not the focus of the model. However, from our phase diagram we are able to identify two distinct regions of spreading behavior (demarcated by the dashed line in Figure 4B) - low values of force and high Arp2/3 concentrations lead to nonisotropic spreading behavior (blue circles). Increasing concentrations of Arp2/3 with a

corresponding increase in force lead to isotropic spreading behavior (red asterisks). From these data, it appears that the interaction between branching reactions and membrane force is a key determinant of isotropic spreading.

These results suggest that the effects of membrane resistance forces integrated with the biochemical reaction machinery can lead to macroscopic cellular behavior. The response to varying membrane resistance force may be indicative of the operational range for the force dependent feedback loop, where the growing filament network exerts outward pressure on the plasma membrane while the membrane resistance force in turn affects the branching rates of the actin filaments. In the case of this minimal model with three biochemical reactions, the inclusion of force as an essential component is required to recapitulate experimentally observed behavior.

Effect of capping filament growth

Capping protein concentration affects the cytoskeletal reorganization dynamics by capping the growing barbed ends of actin filaments and preventing further filament elongation. The observed cell spreading rate should represent a balance between the capping and growing rates. The availability of a pharmacologic agent, cytocholasin D that binds to the barbed ends and blocks filament growth allowed us to develop a prediction from the simulations that could be explicitly tested experimentally. We ran a series of simulations, at varying concentrations of capping protein, calculated the mean spreading velocity around the cell periphery and plotted this value against the concentrations of capping proteins used in the simulations. We observed a linear relationship between the decrease in mean spreading velocity around the periphery and

increasing concentration of capping protein (Figure 5A). We then tested if this linear relationship could be observed experimentally. For this, we conducted a set of experiments to measure mean spreading velocity in the presence increasing concentrations of cytochalasin D. The experiments also showed an inverse linear relationship between mean spreading velocity and Cytocholasin D concentration (Figure 5B). To determine if the simulations had essentially captured the balance between the branching, elongation, and capping reactions in the cell we compared the slopes of the two fitted lines (Figure 5C). Both lines showed a slope of 0.82, although the fit for the simulations (R^2~ 0.98) was better than the fit for the experiments (R^2 ~0.85). From this comparative analysis, we conclude that our simplified model consisting of force-constrained three biochemical reactions distributed in space and time can reasonably account for isotropic cell spreading.

Discussion

An important issue in systems biology is the development of biochemical models with appropriate level of detail to explain complex cellular behavior. Given the vast amount of data in the literature it is possible to build very large and detailed models. While such models can and do provide useful information about the underlying complexity of cellular processes, they are not useful in defining the role of the core biochemical events that control complex cellular processes. This is especially true in cases where stochastic biochemical processes give rise to cellular behavior that appears to be largely deterministic. In this study, we have built on previously successful attempts to model aspects to cellular motility (2, 4, 6, 8, 14-16) to define and understand how coupled

biochemical reactions lead to complex cellular behavior. The availability of quantitative experimental data on dynamic cellular behavior was critical to obtain constraints necessary for the development of this temporal model in three spatial dimensions.

The model indicates that a relatively simple set of reactions near the cell surface, in this case actin branching, elongation and capping reactions when constrained by a defined membrane force can yield isotropic spreading. This observation implies that intrinsically stochastic processes can yield deterministic output by the imposition of few (in this case 3) constraints. The spreading process is inherently stochastic because actin filaments can grow in all possible outward directions. This can lead to large fluctuations in the spreading velocity around the periphery. However, the balance of the branching, growing and capping reactions coupled with the resistance force results in similar velocities around the periphery resulting in the largely deterministic behavior observed both in the experiments and simulations. The interplay between the three reactions and total resistance force can be depicted as a set of partially nested feedback loops (Figure 6) that gives rise to a balance that produces similar spreading velocity around the periphery of the cell. It should be noted that the activity levels of the three constraining factors in this model: activated Apr2/3, activated capping protein and activity generated force are all regulated by intracellular signaling networks. Interaction of the cell surface integrin receptors with substrate is known to stimulate force generation (17-20) as well as activate an intracellular signaling network that regulates the activity of Arp2/3 as well as capping protein (Figure 6). This ability of contact originated intracellular signals to control the two opposing reactions by regulating the activity state of branching proteins and capping proteins provides the constraint needed to restrict the trajectories the system can take due

to stochastic nature of the branching reaction. Thus, the ability of signaling networks to impose constraints on intrinsically stochastic processes can be thought of as an important design principle by which the cell can achieve dynamic stability.

Model Development

A three dimensional stochastic model for cell spreading on a fibronectin coated glass slide (Figure S2) was developed. At its core, the model consists of three biochemical reactions, representing the dynamics of actin filaments: (i) actin polymerization, (ii) capping of growing actin filaments and (iii) branching of existing actin filaments (Figure 1a). Overall, the model consists of four parts:

- Filament network – This module forms the basis of the actin filament network at the leading edge. This is shown schematically in Figure 1b. The network is initialized as a set of spatially homogeneously distributed seeding filaments consisting of one Arp2/3 and two actin monomers. The filaments in this module are initiated and connected with other filaments by branches originating from Arp2/3 binding sites on the actin filament. The dynamic growth of this network is modulated by the iterative occurrences of the three reactions as specified by a modified Gillespie's algorithm (21).
- Cell surface – The cell surface is represented by a series of adjacent triangular polyhedrons (Figure 1c(i)) enclosed by a triangulated surface embedded in a three dimensional space, resulting in a triangularized sphere (Figure 1c(ii)), which is similar to the experimentally observed round fibroblast cell as it starts spreading on the fibronectin coated glass surface (Figure 1c(iii)). As the underlying filament reactions progress, the cell surface is actively updated, such that dynamics of the filament network directly changes the location of the cell surface and thus representing the experimentally observed movement of the leading edge.

- Stochastic reaction machinery: We use a modified version of Gillespie's algorithm (21) to simulate the filament reactions stochastically. A dynamic dependency graph is used to describe the logical dependencies between filament reactions (Figure S3). For example, when a filament branching reaction occurs, a new growing filament is created, which in turn leads to three new reactions being associated with the filament. During the simulation, the dynamic dependency graph keeps track of the dependency of each filament reaction on other filament reactions, and updating the status of the affected filament reactions. Since each filament gets updated only when it has to, the algorithm efficiently computes a large and dynamic reaction system.
- Force dependent filament growth: The growth of actin filaments encounters resistance from the plasma membrane (6, 22). The force used in the simulation characterizes the resistance imposed on actin filaments when they grow. This can be interpreted as the force generated from the change of the surface shape of cell membrane by filament growth. The cell membrane is connected with the ends of intracellular cytoskeleton so that the change of cell membrane will cause these connections to generate friction force. The resistance force encountered by the growing filaments directly affects the biochemical kinetics and hence filament dynamics. Mogilner and Oster (14) defined a relationship between the resistance force exerted by the membrane and the biochemical rate constants for the filament dynamics reactions to determine effective rate constants. In our model, we use these effective rate constants for all the three biochemical reactions. The resistance force during polymerization and capping is imposed on the preexisting filament while the resistance force during branching is imposed on the newly formed filament. This force dependent regulation of the

biochemical kinetics results in feedback control of the minimal cell motility machinery. The effective rate constant is given by

$$k_{on}^{'} = k_{on} e^{-(\frac{f\delta}{k_B T})} \qquad (1)$$

where δ is the length increment of actin filament due to addition of one monomer, k_B is the Boltzmann's constant, T is the absolute temperature in Kelvin, and f is the resistance force.

These four modules were implemented in an object oriented simulation program written in C++ on a Linux platform. The custom code was run on a sixteen node Microway Beowulf cluster with Intel Xenon processors. We also used the IA64 system at the San Diego Supercomputing Center for the parameter variation simulations. The motile cell simulation unit consists of three component modules: actin filament network, cell surface topology and the filament reaction events. These three modules were integrated into a unified Monte Carlo simulation based on the modified Gillespie's method (21). The detailed framework of the simulation program is presented in Figure S4. In the simulation algorithm (Figure S3), the initiation step sets up the initial structure of the actin filament network, cell surface and the reaction simulator. The iterative steps follow the status of all the components and update them at each step. The simulation is terminated when one of the following three events occur: maximum time is reached, maximum iteration number is reached, or when no more filament reactions occur because of filament capping. Generally, we were unable to run the simulations beyond one minute of cell spreading. The simulation was carried out for different initial concentrations of actin and its regulators Arp 2/3 and capping protein and different levels of membrane resistance force.

A table of rate constants, initial concentrations, reaction probabilities, the sources of these values and underlying assumptions are provided in Table S1 in the Supplementary Materials. The dependence of spreading on the number of free actin barbed ends was tested using the fungal toxin cytochalasin D (CD). Cytochalasin was added 30 minutes prior to spreading at the indicated concentration. Spreading assays were carried out as described previously (1).

ACKNOWLEDGEMENTS

This research was supported in part by NIH grant GM 072853 and the Nanomedicine Center Development Grant EY016586 and by the National Science Foundation through TeraGrid resources provided by the San Diego Supercomputing Center.

REFERENCES

1. Dubin-Thaler, B. J., Giannone, G., Dobereiner, H. G. & Sheetz, M. P. (2004) *Biophys J* **86,** 1794-1806.
2. Mogilner, A. & Rubinstein, B. (2005) *Biophys J* **89,** 782-795.
3. Bohnet, S., Ananthakrishnan, R., Mogilner, A., Meister, J. J. & Verkhovsky, A. B. (2006) *Biophys J* **90,** 1810-1820.
4. Mogilner, A. & Edelstein-Keshet, L. (2002) *Biophys J* **83,** 1237-1258.
5. Grimm, H. P., Verkhovsky, A. B., Mogilner, A. & Meister, J. J. (2003) *Eur Biophys J* **32,** 563-577.
6. Mogilner, A. & Oster, G. (2003) *Biophys J* **84,** 1591-1605.
7. Dawes, A. T., Bard Ermentrout, G., Cytrynbaum, E. N. & Edelstein-Keshet, L. (2006) *J Theor Biol* **242,** 265-279.
8. Edelstein-Keshet, L. & Ermentrout, G. B. (2001) *J Math Biol* **43,** 325-355.
9. Civelekoglu, G. & Edelstein-Keshet, L. (1994) *Bull Math Biol* **56,** 587-616.
10. Dobereiner, H. G., Dubin-Thaler, B. J., Hofman, J. M., Xenias, H. S., Sims, T. N., Giannone, G., Dustin, M. L., Wiggins, C. H. & Sheetz, M. P. (2006) *Phys Rev Lett* **97,** 038102.
11. Svitkina, T. M., Bulanova, E. A., Chaga, O. Y., Vignjevic, D. M., Kojima, S., Vasiliev, J. M. & Borisy, G. G. (2003) *J Cell Biol* **160,** 409-421.
12. Giannone, G., Dubin-Thaler, B. J., Rossier, O., Cai, Y., Chaga, O., Jiang, G., Beaver, W., Dobereiner, H. G., Freund, Y., Borisy, G., *et al.* (2007) *Cell* **128,** 561-575.
13. Dobereiner, H. G., Dubin-Thaler, B., Giannone, G., Xenias, H. S. & Sheetz, M. P. (2004) *Phys Rev Lett* **93,** 108105.
14. Mogilner, A. & Oster, G. (1996) *Biophys J* **71,** 3030-3045.
15. Ermentrout, G. B. & Edelstein-Keshet, L. (1998) *Bull Math Biol* **60,** 477-503.
16. Peskin, C. S., Odell, G. M. & Oster, G. F. (1993) *Biophys J* **65,** 316-324.
17. Jiang, G., Huang, A. H., Cai, Y., Tanase, M. & Sheetz, M. P. (2006) *Biophys J* **90,** 1804-1809.
18. Ingber, D. E. (2006) *Faseb J* **20,** 811-827.
19. Ingber, D. E. (1997) *Gravit Space Biol Bull* **10,** 49-55.
20. Ko, K. S. & McCulloch, C. A. (2001) *Biochem Biophys Res Commun* **285,** 1077-1083.
21. Gillespie, D. T. (1977) *J Phys Chem* **81,** 2340-2361.
22. Raucher, D. & Sheetz, M. P. (1999) *Biophys J* **77,** 1992-2002.

Figure Legends

Figure 1: Simulational framework for isotropic cell spreading

Figure 1a: Schematic of the three main reactions that affect the actin filament network. Addition of a monomer increases filament length via polymerization. Filament branching is caused by binding of the Arp2/3 complex to the pre-existing filament. Capping protein caps a pre-existing filament and prevents further polymerization and filament elongation.

Figure 1b: Cross-section of the simulational cell and the cortex. Inset shows a section of the cortex with a highly branched actin filament network.

Figure 1c: Model geometry for the biochemical reactions shown in Figure 1a. A bright field image of a fibroblast as it enters the isotropic spreading stage is used as the framework for the representation of a sphere 2 μm in diameter. In order to implement the biochemical reactions in the spatio-temporal domain, the sphere is converted to a triangularized sphere.

Figure 2: Spatio-temporal distribution of spreading velocity

Figure 2a: Cell spreading velocity obtained from simulations: The heat map shows the average velocity distribution over 24 separate stochastic simulations. The angular velocity distribution over segments of 10° is followed in time for one minute (60 s). Velocity is shown in μm/min. The concentrations of actin, Arp2/3 and capping protein used are 20 μM, 0.04 μM and 0.04 μM respectively.

Figure 2b: Experimentally determined spreading velocity distributions. The heat map for the experimentally measured velocity is obtained using TIRF imaging at 2 second interval during isotropic spreading (1).

Figure 2c: Velocity distribution across the cell periphery at 5, 10, 20 and 40 seconds from simulations. The mean edge velocity is denoted by the dotted line. Isotropic spreading behavior is seen at 20 and 40 seconds.

Figure 2d: Velocity distributions similar to Figure 2c from experiments.

Figure 3: Effect of Arp2/3 concentration on isotropic cell spreading

Spatio-temporal velocity distributions in response to changing Arp2/3 concentrations. The different values of Arp2/3 studied are (A) 0.02, (B) 0.08, (C) 0.16 μM. Actin and capping protein concentrations are maintained at 20 and 0.04 μM respectively and the membrane resistance force is maintained at 500 pN/μm^2. Changing Arp2/3 concentrations leads to a change in the range of velocities attained and their distribution. As Arp2/3 concentration increases fewer points of negative velocity (or retraction) are observed.

Figure 4A: Effect of membrane resistance force on spreading velocity distribution

The effect of changing the membrane resistance force is tested for Arp2/3 concentration of 0.08 μM. The actin and capping protein concentration are maintained at 20 and 0.04 μM. The membrane resistance is varied from 0 to 1000 pN/μm^2. As the membrane resistance force increases, the spreading velocity decreases. The velocities are averaged from 12 individual runs and the averages are shown. Yellow indicates zero in the heat maps.

Figure 4B: Phase plot of isotropic versus non-isotropic cell spreading

Based on experimental observations, we define isotropic spreading as the spreading event where the standard deviation of average peripheral velocity is less than 20% of the mean. We see isotropic spreading behavior for low values of force and Arp2/3 and as the concentration of Arp2/3 increases, we need higher values of force to observe isotropic spreading. The dashed line suggests demarcation of the force/Arp2/3 plane where isotropic to non-isotropic transition occurs in the cases we have tested.

Figure 5: Effect of capping protein concentration on spreading velocity distribution

Figure 5A: Mean velocity around the cell periphery is plotted as a function of varying capping protein concentrations. For these simulations the concentration of actin was 20 μM and Arp2/3 0.16 μM and force 500pN/μm^2. Each point represents mean velocity from 24 simulations. Coefficient of variance was under 20%.

Figure 5B: The mean spreading velocity in response to increasing cytochalasin D concentration show a similar decreasing trend to increasing concentrations of capping protein.

Figure 5C: Regression analysis shows a linear dependence of normalized concentration of capping protein in simulations and cytochalasin D in experiments with correlation coefficients of 0.98 and 0.85 respectively. The slope of the fitted line was -0.82.

Figure 6: Regulatory loops in the minimal machinery involved in isotropic cell spreading.

The minimal simulation machinery that is required to capture the spatio-temporal distribution of the spreading velocity of a cell undergoing isotropic spreading is summarized in this flow chart. The biochemical reactions polymerization, capping, and branching interact to modulate the cell surface, filament density, resistance force and spreading velocity in both positive and negative interactions. The connector with arrow end denotes positive interaction and the connector with line end denotes negative interaction. The concentrations of capping protein and Arp2/3 complex are regulated by integrin mediated signaling from the cell surface to the cytoskeleton.

Table 1: Variation of force, Arp2/3 and capping protein studied in the model along with the mean velocity and deviation to identify conditions that lead to isotropic spreading behavior.

Force ($pN/\mu m^2$)	Arp2/3 (μM)	Capping (μM)	mean velocity (μm/min)	SD	% deviation	Isotropic
0	0.02	0.04	2.03	0.37	18.23	yes
0	0.08	0.04	1.2	0.3	25.00	no
0	0.16	0.04	0.011	0.005	45.45	no
30	0.02	0.04	1.45	0.23	15.86	yes
30	0.08	0.04	0.93	0.26	27.96	no
30	0.16	0.04	0.68	0.523	76.91	no
100	0.02	0.04	0.988	0.13	13.16	yes
100	0.08	0.04	0.89	0.18	20.22	no
100	0.16	0.04	0.012	0.0026	21.67	no
300	0.02	0.04	0.65	0.14	21.54	no
300	0.08	0.04	0.7	0.113	16.14	yes
300	0.16	0.04	0.65	0.131	20.15	no*
500	0.02	0.04	0.35	0.03	9.43	yes
500	0.04	0.04	0.39	0.05	11.79	yes
500	0.08	0.04	0.39	0.05	12.82	yes
500	0.16	0.04	0.39	0.07	16.67	yes
500	0.16	0.04	0.39	0.06	16.41	yes
1000	0.02	0.04	0.37	0.133	35.95	no
1000	0.08	0.04	0.48	0.07	14.58	yes
1000	0.16	0.04	0.55	0.1	18.18	yes

*- the percentage is 0.15% more than cutoff, can be considered to be isotropic.

Figure 1

(A)

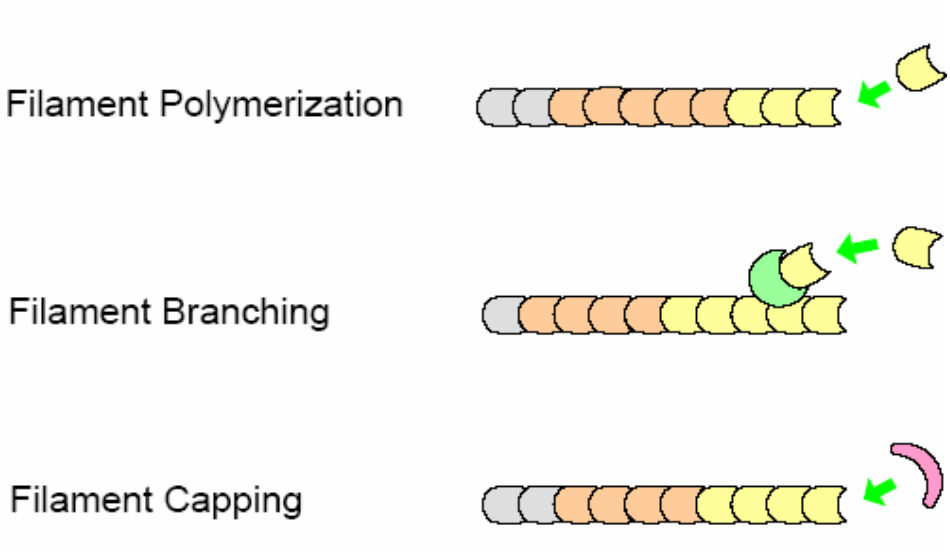

(B)

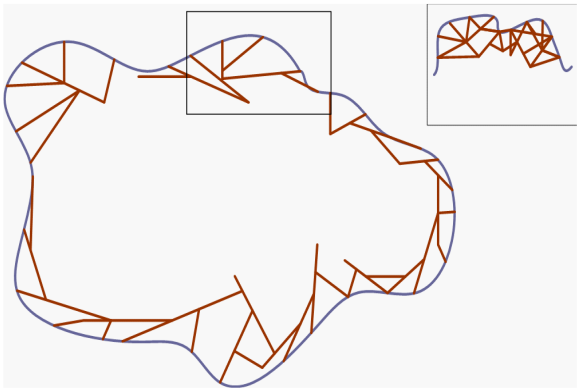

(C)

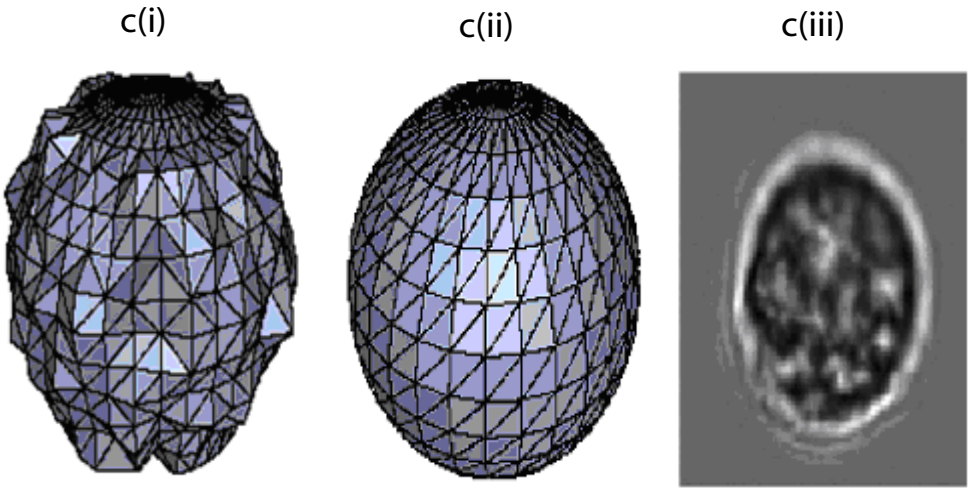

Figure 2A : Simulation

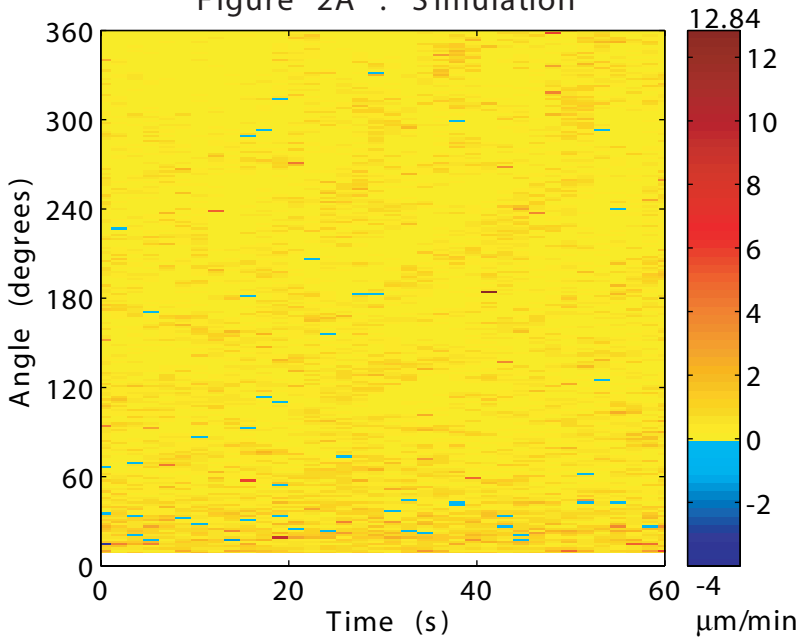

Figure 2B : Experiment

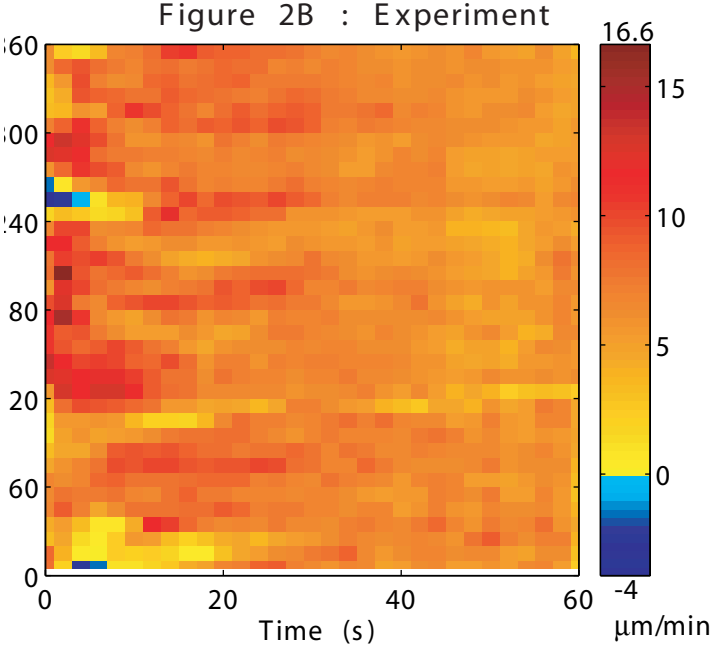

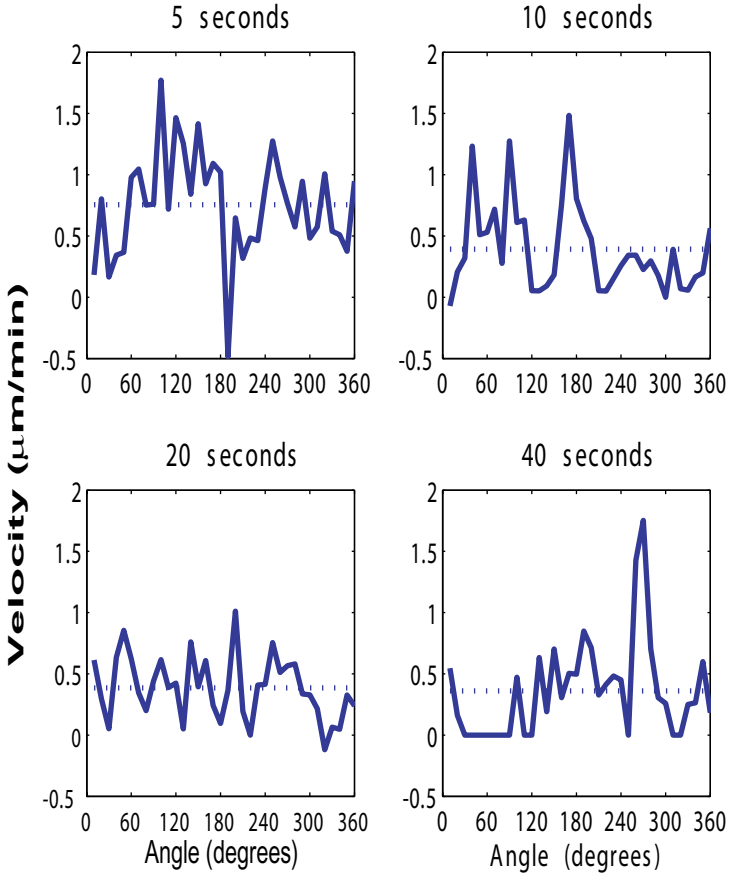

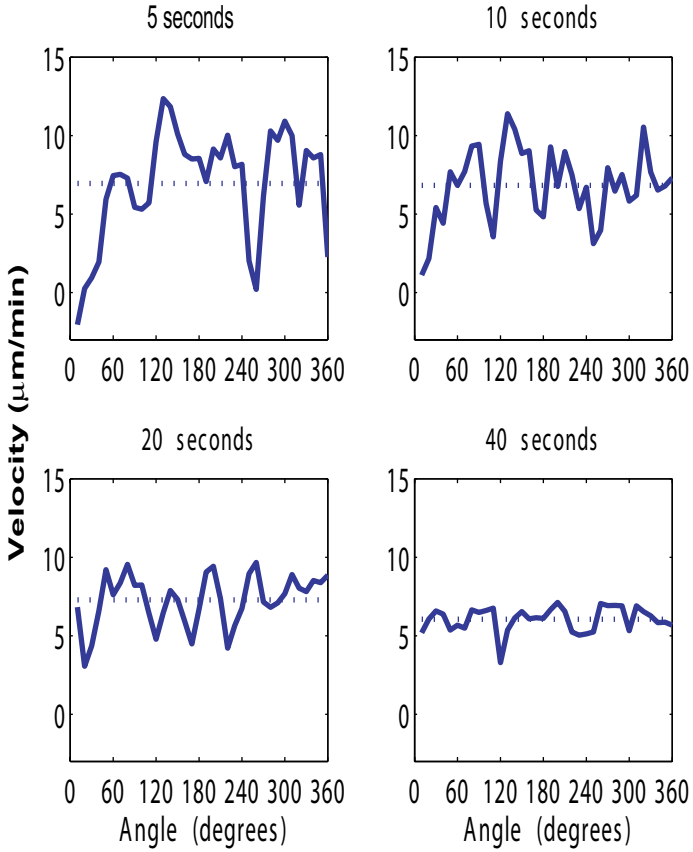

Figure 3

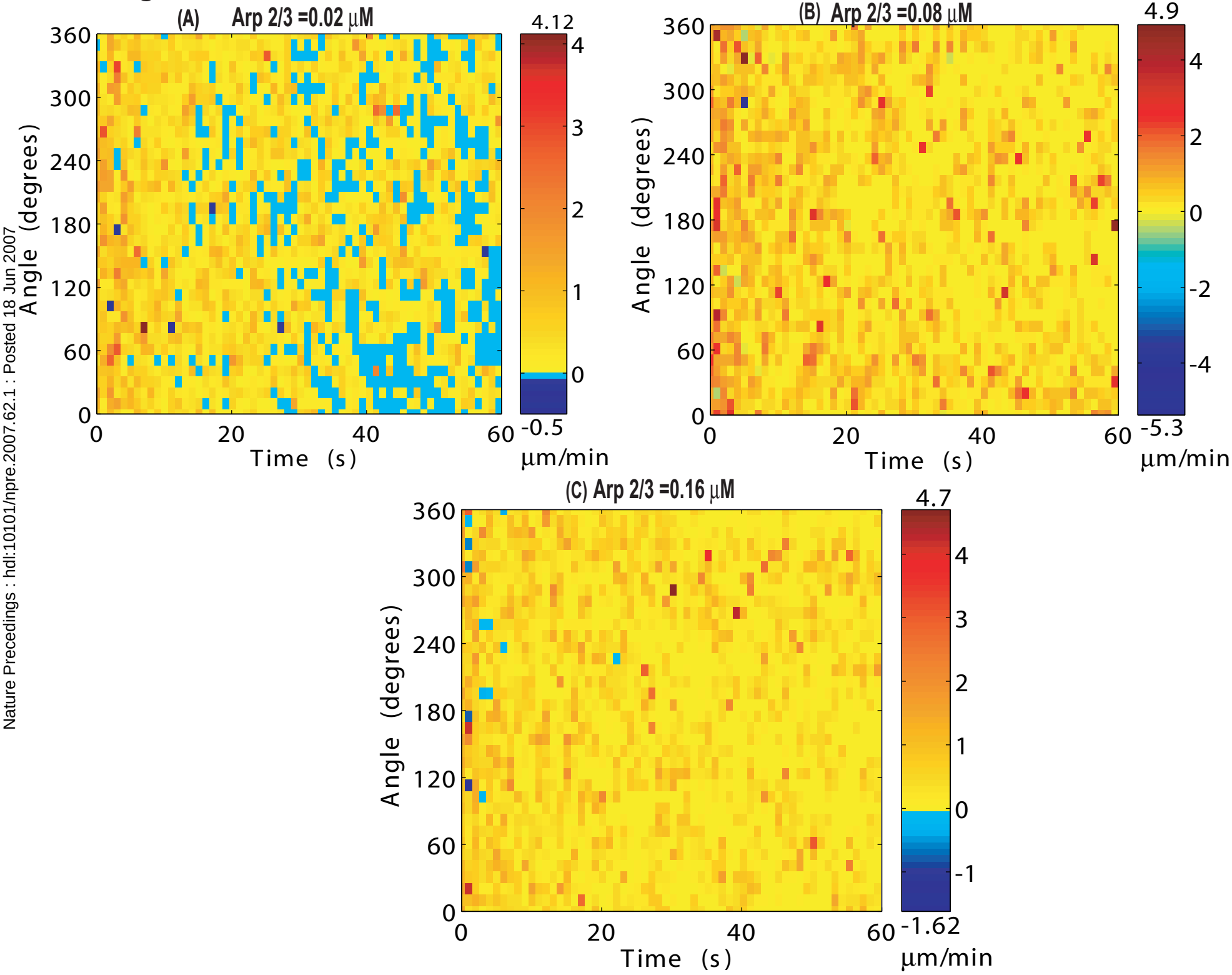

Figure 4A

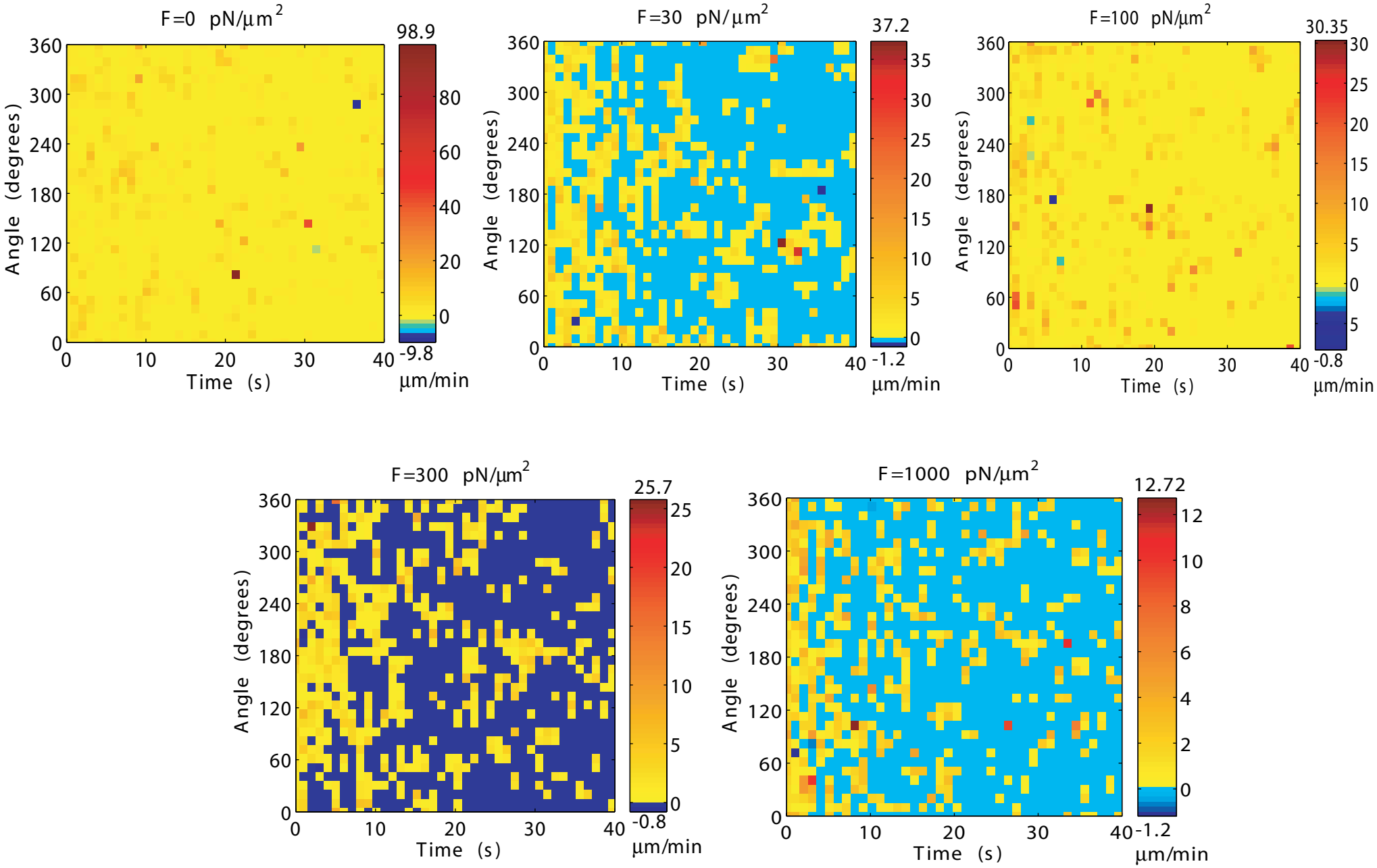

Figure 4B

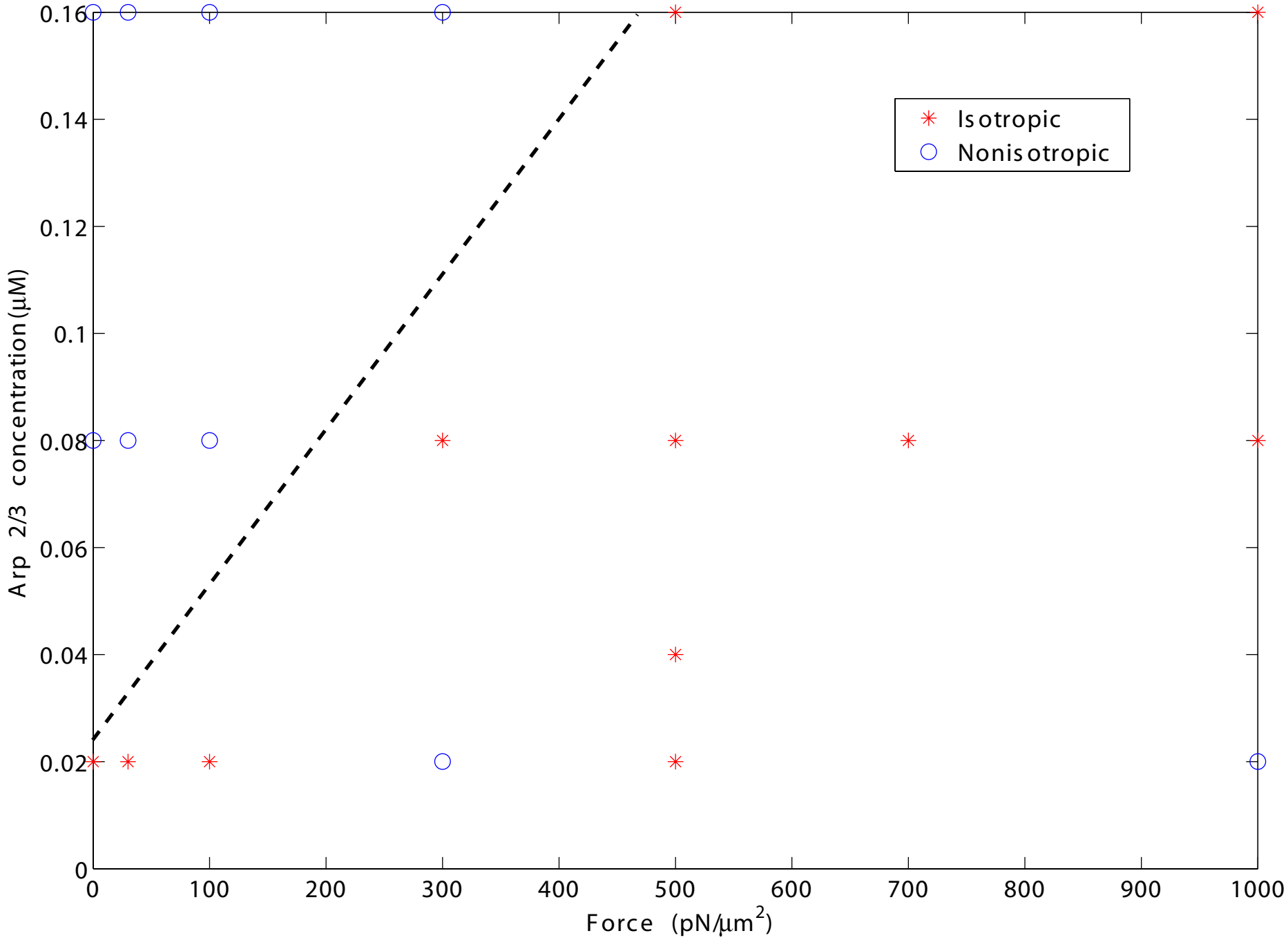

Figure 5

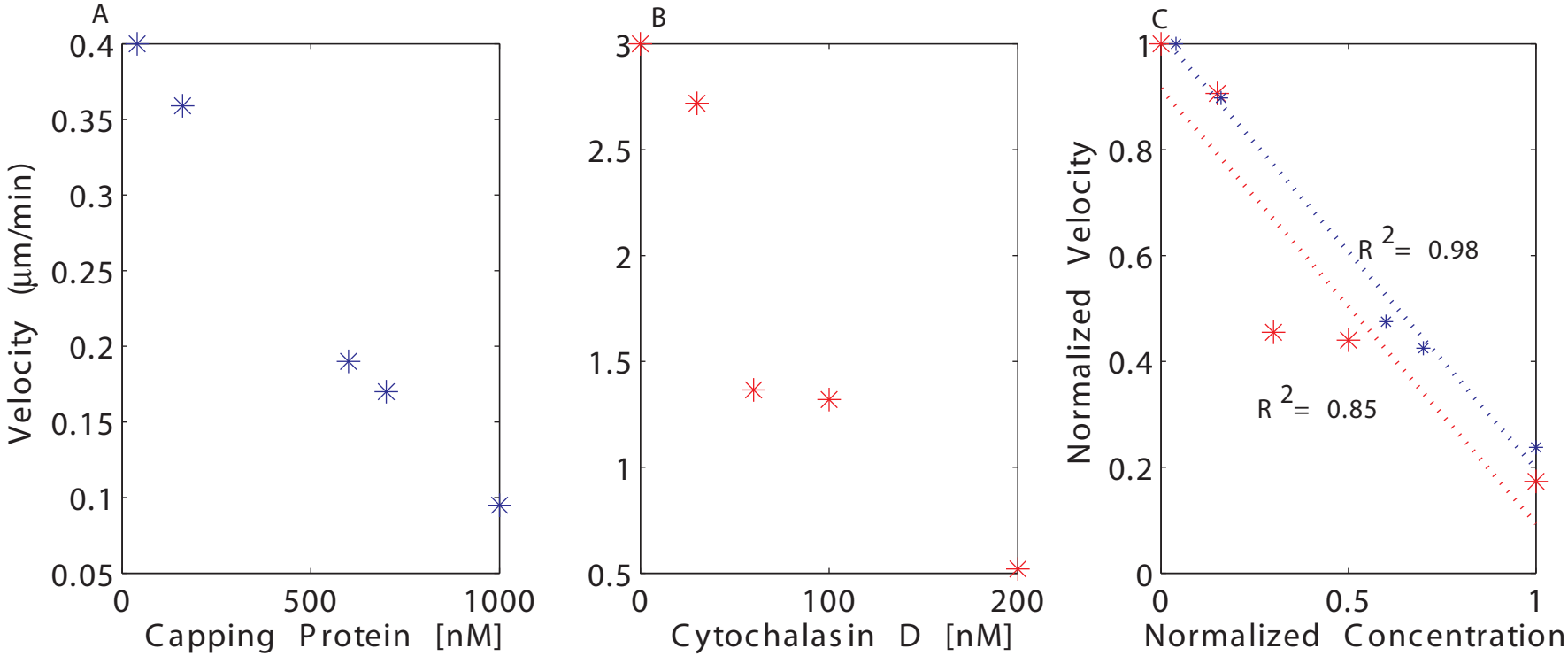

Figure 6

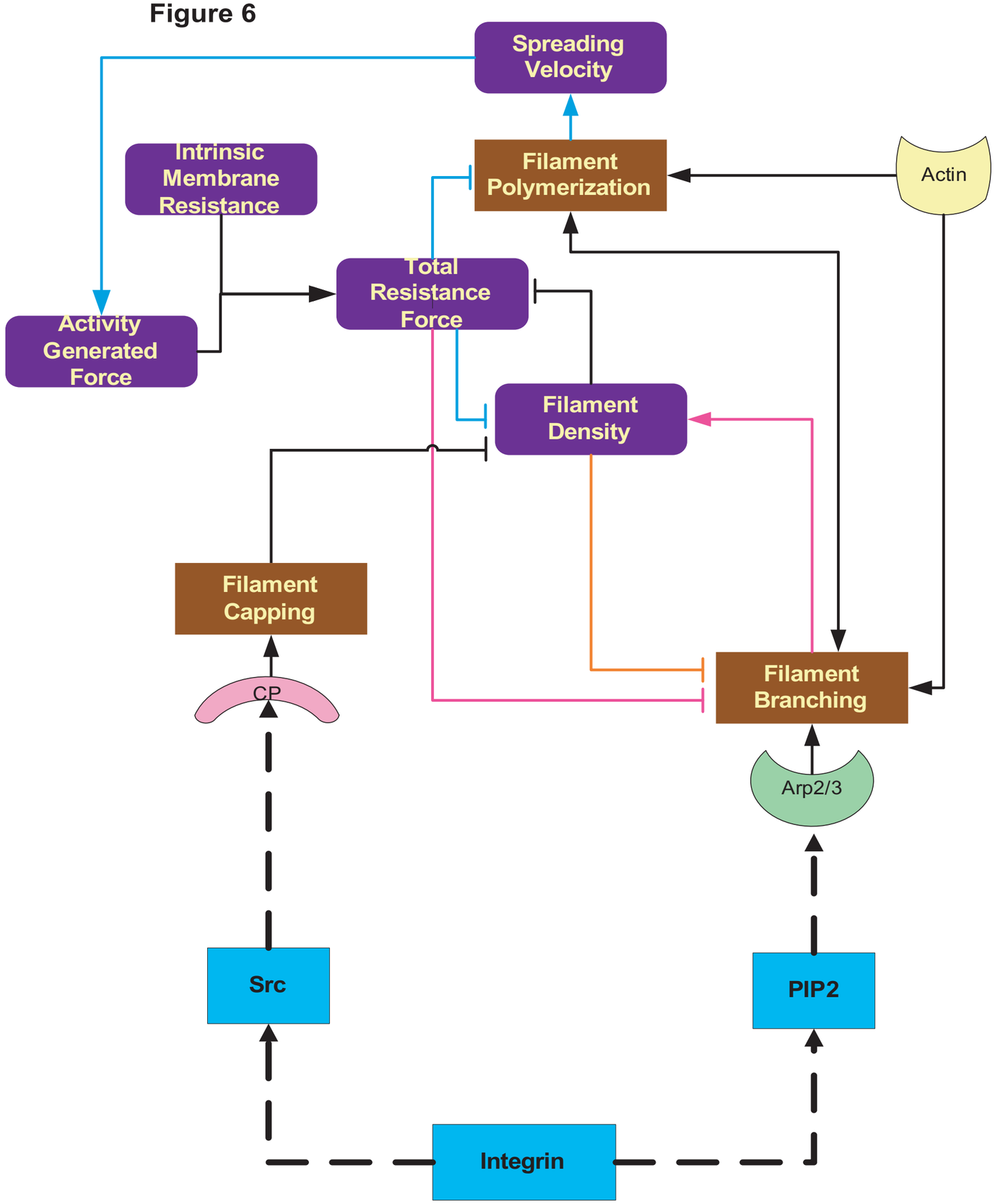

Supplementary Material

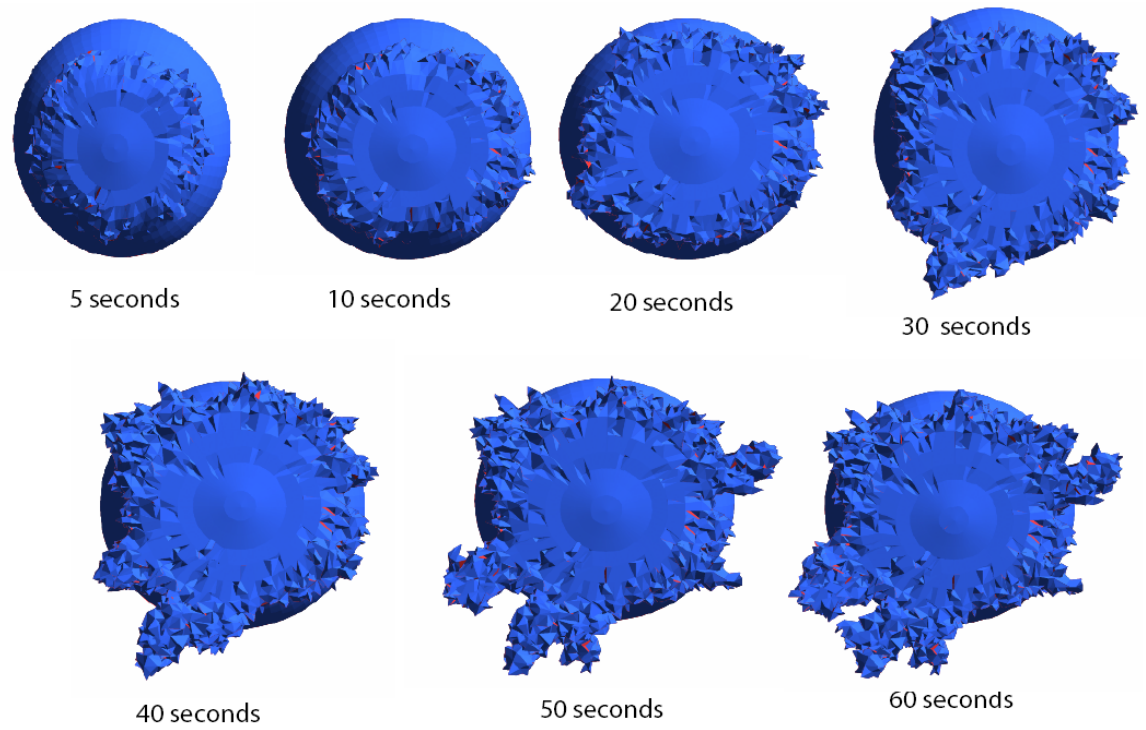

Figure S1: Snapshots of a spreading cell at different times

The spreading cell was rendered using an .off file viewer based on the numerical simulations. The actin, Arp2/3 and capping protein concentrations were 20, 0.04, 0.04 μM respectively and the membrane resistance force was 500 pN/μm^2.

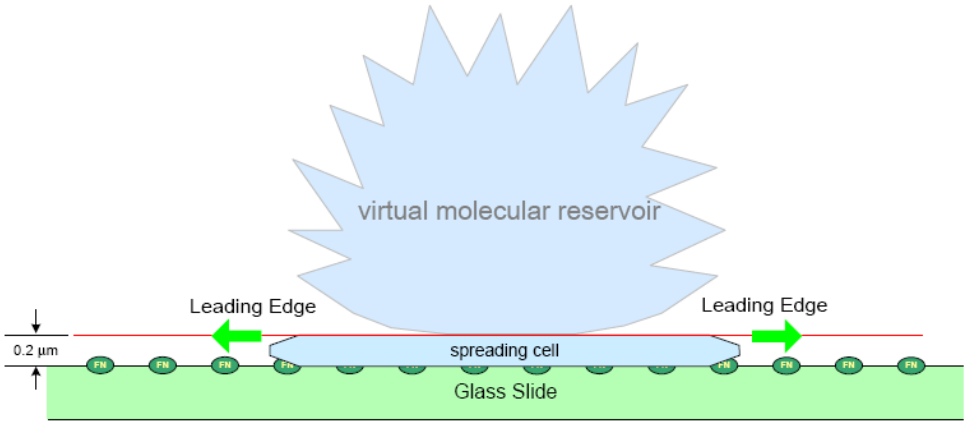

Figure S2: Simulation model of a fibroblast spreading on a fibronectin coated glass slide

In the simulation model, only the bottom portion of a fibroblast cell with a thickness of 0.2 µm can spread and is simulated whereas the rest of the cell does not change. This was done in order to match the leading edge, whose spreading velocity is measured in experiment.

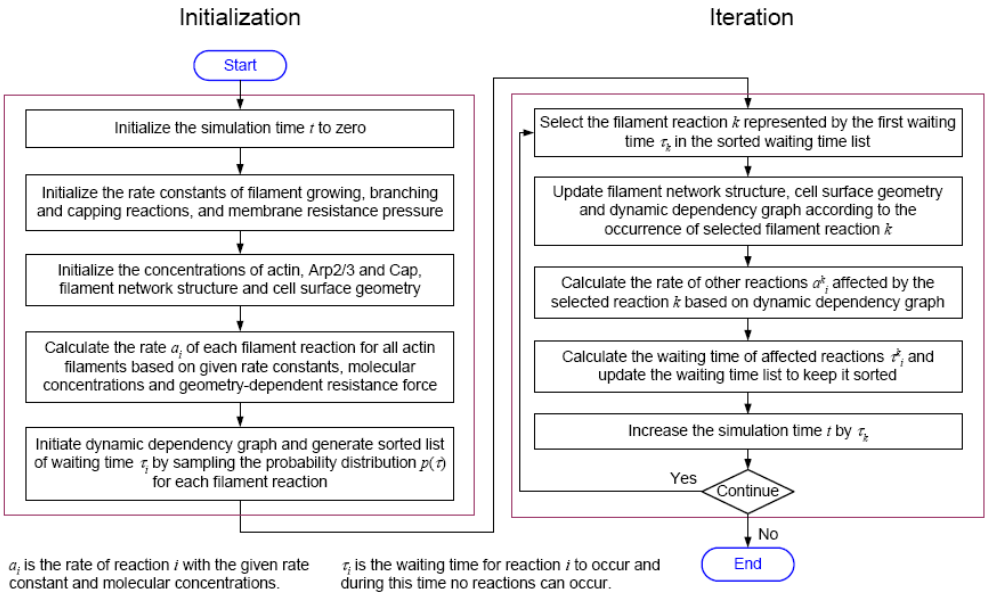

Figure S3: Stochastic algorithm of the simulation program

The stochastic algorithm of the simulation program includes initiation and iteration. The initiation step constructs the structure of initial filament network and the geometry of initial cell surface, calculates the rate of filament reactions, and initializes the dynamic dependency graph and the sorted waiting time list. The iteration step executes the first reaction stored in the sorted waiting time list, updates filament network structure and cell surface geometry, updates the dependency graph and the waiting time list, calculates the rate and the waiting time of all affected filament reactions according to the dynamic dependency graph, and increases the simulation time.

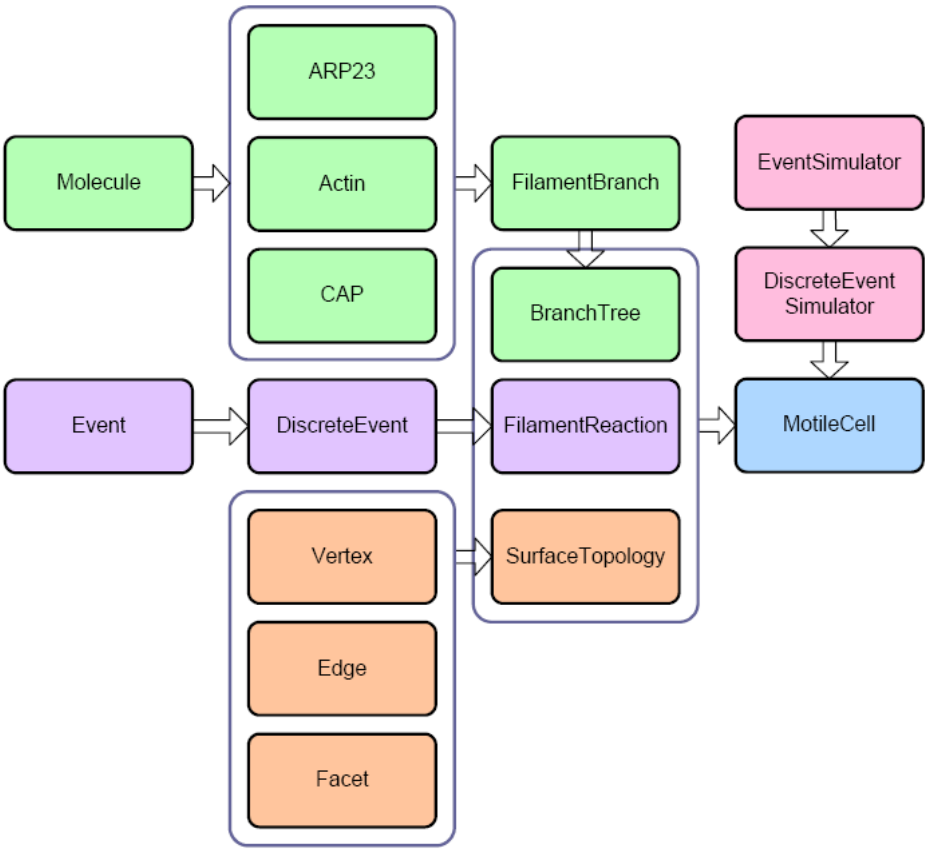

Figure S4: Framework of the simulation program

The framework of the simulation program is composed of four sets of building blocks: the actin filament network denoted by the green blocks, the cell membrane surface denoted by the orange blocks, the filament reaction event denoted by the purple blocks, and the discrete event simulator denoted by the pink blocks. All these components are integrated into the motile cell block in blue color.

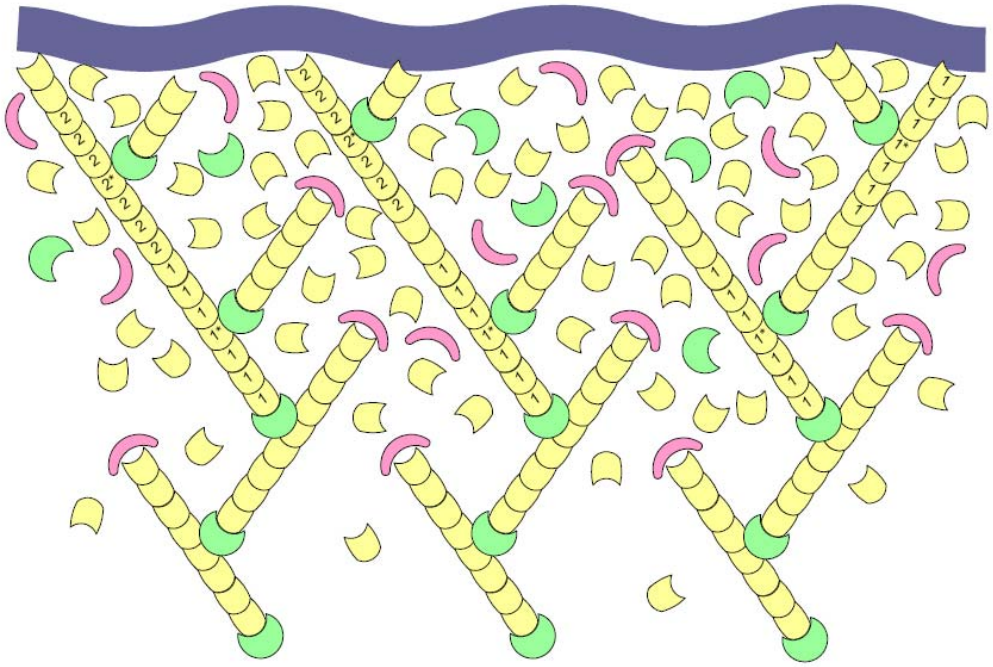

Figure S5: Spatial constraints on filament branching

Filament branching reaction is limited by the spatial hindrance from the filament branches created on the same existing filament. Because the number of polymerized actin monomers on existing filament to which Arp2/3 protein binds is 7 as listed in Table 4.1, no new filament can be created if there are not enough actin monomers on existing filament available for Arp2/3 binding. The left filament tree shows two new filaments are created next to each other, the middle filament tree shows two new filaments are created with some distance, and the right filament tree shows only single filament is created on existing filament because of the lack of available polymerized actin monomers on existing filament.

Table S1 : Input Parameters

No.	Parameter	Value	Units	References
1	**Rate constant of filament polymerization**	11.6	$\mu M^{-1}s^{-1}$	(1)
2	**Diameter of Actin Monomer**	5.5	nm	(2)
	Although the diameter of individual actin monomer is 6 nm, the distance between neighboring actin monomers in actin filament is 5.5 nm due to the double helix structure of polymerized actin filament (2). Since the purpose of using this parameter is to determine the length increment of actin filament caused by filament polymerization reaction, the model assumes the diameter of actin monomer to be 5.5 nm.			
3	**Diameter of Arp2/3 protein**	15	nm	(3)
	High-resolution experiment reveals the crystal structure of Arp2/3 protein complex and determines its dimensional size around 7 to 15 nm (3). The model uses the 15 nm as the diameter of Arp2/3 protein.			
4	**Diameter of capping protein**	10	nm	Estimated
	The diameter of capping protein is not known yet and must be estimated. Since capping protein is known to be a small molecule, the model assumes that it is smaller than Arp2/3 protein. And because capping protein can bind to the barbed end of double-helix actin filament, it implies that capping protein should be able to cover the size of two actin monomers. Therefore, the model assumes that the diameter of capping protein is 10 nm.			
5	**Filament branching angle**	70°		(4)
6	**Number of nucleated monomers**	2		(5)
	This is the number of polymerized actin monomer in the initial actin filament nucleated by Arp2/3 protein in filament branching reaction. Based on the subunit structure of Arp2/3 protein, previous study suggests that the binding of two actin monomers to Arp2/3 protein be the initial step of			

creating a new actin filament (5).

7	**Number of monomers binding Arp2/3** This parameter describes the number of polymerized actin monomers on an existing filament that bind Arp2/3 during filament branching. (6) shows that the binding site of Arp2/3 on the existing filament covers about 6 to 7 polymerized actin monomers.	7		(6)
8	**Resistance pressure from membrane** This is the average resistance force imposed on growing actin filament by unit area of cell membrane. This parameter is estimated from previous computational study (7) where the resistance pressure used ranges from 50 to 200 pN/μm on a 0.17-μm thick lamellipodium which corresponds to 300 to 1100 pN/μm^2. Because fibroblast cell is capable of buffering this resistance force with membrane reservoir during cell spreading (8), the model selects a constant intermediate value 500 pN/μm^2 for membrane resistance pressure. We also vary the value of force in the model in the range 0 to 1000 pN/μm^2.	500	pN μm^{-2}	(7)
9	**Thickness of the leading edge** For the fast membrane protrusion involved in cell spreading or cell migration, the leading edge of cell membrane is usually like a flatted sheet and its thickness has been well measured (9).	200	nm	(9)
10	**Initial cell diameter** The value of this parameter is estimated directly from experiments where single fibroblast cell has spherical shape before it is dropped onto the glass slide coated with fibronectin signaling molecules. The initial diameter of spherical fibroblast cell is about a few microns before it starts spreading on glass slide. So the model assumes the initial cell diameter to be 2 μm as illustrated in Figure 4.2.	2	μm	Estimated from experiment
11	**Thickness of the cortical region**	50	nm	Estimated

The filament network at the very leading edge is cross-linked by highly branched and short filaments whereas the filament network inside cell is usually formed by straight and long filaments (10). Since this model only studies the actin dynamics of branched filament network, the model confines all filament reactions within the 50-nm cortical region underneath cell membrane.

12	**Initial number of actin filaments**	2000		Estimated

The initial filament density was chosen so that it would be sufficient to initiate cell spreading. After being tested with various values, we decided to use 2000 actin filaments evenly distributed on spherical cell as the starting point of cell spreading simulation.

13	**Thermodynamic constant k_BT**	4.1	pN.nm	Calculated

Calculated at 300 K, where k_B is the Boltzmann constant

14	**Rate constant of filament branching**	1.25	$\mu M^{-3}s^{-1}$	Estimated

Because of the highly branched structure of filament network at the leading edge of spreading cell, filament branching reaction is known to be very fast during cell spreading process. Since filament branching reaction is a fourth-order reaction and the concentration of actin monomer is assumed as 20 μM, the model selects 1.25 $\mu M^{-3} \cdot s^{-1}$ as the rate constant of filament branching reaction such that the reaction rate remains moderately high (ranges between 10 to 100 reactions per second).

15	**Rate constant of filament capping**	35	$\mu M^{-1}s^{-1}$	Estimated

Since the binding affinity of capping protein to the barbed end of actin filament is known to be high and the rate of filament capping reaction should match the rate of branching reaction during cell spreading, the model assumes the rate constant of capping reaction to be 35 $\mu M^{-1} \cdot s^{-1}$ such that the rate of branching reaction is comparable with but a little smaller than the rate of branching

reaction (ranges between 0.35 to 70 reactions per second).

16	**Arp 2/3 initial concentration**	0.04	μM	(11)
	Variations used in the simulation are 0.02, 0.08 and 0.16 μM			
17	**Capping protein initial concentration**	0.04	μM	(11)
	Variations used in the simulation are 0.32, 2.56 μM			
18	**Actin initial concentration**	20	μM	Estimated
	A rough estimation based on the published measurements of actin filament dynamics in fast migrating fibroblast cell (9) shows that in order to achieve the polymerization rate of 97±16 monomers per filament per second at the condition of 1370±578 growing filaments at the leading edge of lamellipodium, suggesting that the concentration of actin monomer at the leading edge ranges from 8 to 15 μM assuming the resistance pressure of cell membrane is 500 pN/μm^2 (7). Considering other resistance factors to the polymerization rate constant, the model assumes that the concentration of actin monomer at the leading edge is 20 μM.			

REFERENCES

1. Pollard, T. D., Blanchoin, L. & Mullins, R. D. (2000) *Annu Rev Biophys Biomol Struct* **29,** 545-576.
2. Howard, J. (2001) *Mechanics of motor proteins and the cytoskeleton* (Sinauer Associates Inc, Sunderland MA).
3. Robinson, R. C., Turbedsky, K., Kaiser, D. A., Marchand, J. B., Higgs, H. N., Choe, S. & Pollard, T. D. (2001) *Science* **294,** 1679-1684.
4. Medalia, O., Weber, I., Frangakis, A. S., Nicastro, D., Gerisch, G. & Baumeister, W. (2002) *Science* **298,** 1209-1213.
5. Higgs, H. N. & Pollard, T. D. (2001) *Annu Rev Biochem* **70,** 649-676.
6. Volkmann, N., Amann, K. J., Stoilova-McPhie, S., Egile, C., Winter, D. C., Hazelwood, L., Heuser, J. E., Li, R., Pollard, T. D. & Hanein, D. (2001) *Science* **293,** 2456-2459.
7. Mogilner, A. & Edelstein-Keshet, L. (2002) *Biophys J* **83,** 1237-1258.
8. Raucher, D. & Sheetz, M. P. (1999) *Biophys J* **77,** 1992-2002.
9. Abraham, V. C., Krishnamurthi, V., Taylor, D. L. & Lanni, F. (1999) *Biophys J* **77,** 1721-1732.
10. Pollard, T. D. & Borisy, G. G. (2003) *Cell* **112,** 453-465.
11. Loisel, T. P., Boujemaa, R., Pantaloni, D. & Carlier, M. F. (1999) *Nature* **401,** 613-616.